PCCP

Accepted Manuscript

ROYAL SOCIETY OF CHEMISTRY

www.rsc.org/pccp

Journal Name

ARTICLE

Connecting Effect on the First Hyperpolarizability of Armchair Carbon-Boron-Nitride Heteronanotubes: Pattern versus Proportion

Received 00th January 20xx,
Accepted 00th January 20xx

DOI: 10.1039/x0xx00000x

www.rsc.org/

Rong-Lin Zhong, [a, b] Hong-Liang Xu*[b] and Zhong-Min Su*[b]

Carbon-boron-nitride heteronanotubes have attracted a lot of attentions because of their adjustable properties and potential applications in many fields. In this work, a series of CA, PA and HA armchair carbon-boron-nitride heterojunction nanotubes models were designed to explore the nonlinear optical (NLO) properties and physical insight into the structure-property relationship, where CA, PA and HA represents the model that is obtained by doping the carbon segment into pristine BNNT fragment circularly around the tube axis, parallel and helically to the tube axis respectively. Results show the first hyperpolarizability (β_0) of the armchair BNCNT models is dramatically dependent on the connecting patterns of carbon/boron nitride fragment. Significantly, the β_0 of PA-6 is 2.00×10^4 au, which is almost two order of magnitude larger than that (6.07×10^2 and 1.55×10^2 au) of HA-6 and CA-6. Besides, the β_0 of PA and CA models increases with the increase of carbon proportion, whereas that of HA-n models shows a different tendency. Further investigations on transition properties show that the curved charge transfer from N-connecting carbon atoms to B-connecting carbon atoms of PA models is the essential origin of the big difference among these models. The new knowledge about armchair BNCNTs may provide important information for the design and preparation advanced NLO nano-materials.

Introduction

The last two decades have already witnessed the progress in the design and preparation of advanced nonlinear optical (NLO) materials due to their widely potential applications in laser field[1-8]. Nowadays, various chemical substances have been proposed as excellent NLO materials such as inorganic crystal materials[9-13], organic molecular materials[5, 7, 8, 14, 15], organic metal complexes[4, 16, 17] and excess electrons compounds[18-23] *et.al.*. It is well known that the inorganic crystal materials have been used for about half a century because of their stable physical and chemical properties. However, the NLO response of inorganic materials is relatively small that limits their potential applications in many fields[3, 8]. In general, the NLO susceptibility of organic materials is remarkably larger than inorganic crystals but the stability of organic molecules is a fatal shortcoming for the applications in laser devices[2, 3]. Recently, the distinctive size effect and conceivable applications in numerous challenging fields promote the increasing number of research interests on nano-materials with exceptional NLO responses[24-27]. It is worthy of note that the NLO properties of carbon nanotubes (CNTs) and boron nitride nanotubes (BNNTs) have been extensively investigated by both experimental[28-31] and theoretical chemists[6, 24, 32].

BNNTs are representative one-dimensional analogous of CNTs and have attracted continuous research interests since they were discovered in 1995[33]. In contrast to the metallic or semiconducting CNTs, BNNTs are known as permanent semiconductors with a wide band gap that is almost independent on the tube chirality and morphology[34-41]. Recently, a series of investigations revealed that the second-harmonic generation response of BNNTs are remarkable, which shows the promising applications in nonlinear optical materials[42-47]. However, the microscopic first hyperpolairizability[8] (β) of BNNT is relatively small due to the wide band gap and inactive electronic properties[34]. On the other hand, recent investigations show that the chirality CNTs exhibit remarkable second NLO response although it is forbidden in centrosymmetric CNTs[24, 25, 31, 32]. During the past decade, an increasing number of investigations have focused on exploring the carbon-boron-nitride heteronanotubes to study the novel structures with adjustable properties[28, 48-56]. Relative studies on the structures and properties of carbon-boron-nitride heteronanotubes have shown that their electronic properties obviously depend on the arrangement and relative proportion of BN and C atoms[40, 57]. In particular, Turner and co-worker demonstrated that the energy gap of the heteronanotubes can be tuned by modifying the C/BN-segments combinations[58]. Correspondingly, our recent study indicates the N-connecting pattern of the BN-segment linking

[a] Institute of Theoretical Chemistry, Jilin University, Changchun, 130023 Jilin, People's Republic of China
[b] Institute of Functional Material Chemistry, Faculty of Chemistry, Northeast Normal University, Changchun, 130024 Jilin, People's Republic of China
hlxu@nenu.edu.cn, zmsu@nenu.edu.cn

Electronic Supplementary Information (ESI) available: The test for basis sets is shown in Electronic Supplementary Information. See DOI: 10.1039/x0xx00000x

to the C-segment is an efficient way to regulate the NLO response of zig-zag heterojunction nanotubes[59-61]. However, the NLO properties of armchair heterojunction nanotubes is rarely reported though they have caught an increasing number of research interests[58, 62, 63].

In this work, we report a quantum chemical investigation on the static first hyperpolairizability (β_0) of a series of armchair carbon-boron-nitride heterojunction nanotubes (BNCNTs) models to reveal the physical insight of the structure-property relationship. As shown in Figure 1, CA, PA and HA represent three isoelectronic models those are obtained by doping the carbon segment into pristine BNNT fragment circularly around the tube axis, parallel and helically to the tube axis. Interestingly, results show that the β_0 value of PA is 2.00×10^4 au, which is dramatically larger than that of CA and HA (1.55×10^2 and 6.07×10^2 au). Besides, the β_0 values of PA models are significantly dependent on the carbon proportion, whereas those of CA and HA models are slightly influenced. The new discovery on the electronic properties of armchair BNCNTs might provide important information for the design and preparation high performance NLO nano-materials in the future.

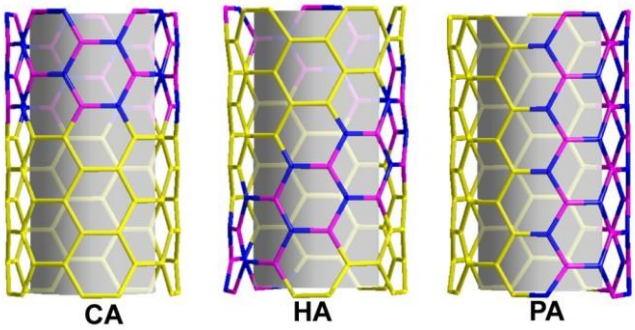

Figure 1. The optimized structure of the three BNCNT ($H_{20}B_{20}N_{20}C_{60}$) models (hydrogen is used as passivated atom on the periphery, which is not shown).

Computational Details

For theoretical investigations, selecting a suitable model is the critical strategy to understand relationship between the calculated results and physical properties[46, 47, 64]. In this work, the carbon-boron-nitride heterojunction nanotube fragment (5, 5) with a suitable length (13 Å) is chosen as the fundamental models. The geometry structures were optimized at the density functional theory (DFT) B3LYP[65, 66]/6-31G(d) level. In this work, the main calculations were based on cluster models in which the atoms on the periphery were saturated by hydrogen atoms. To study the effects of the nanotube termination, we performed a test calculation by considering the one-dimensional periodic boundary conditions (PBC) along the tube axis to simulate infinitely long ternary carbon-boron-nitride heteronanotubes with different carbon proportion (the details about the calculation are shown in ESI). It is worthy of note that the test calculation on the energy gap exhibits consistency between the PBC and cluster models although the energy gap increases 0.29-0.65 eV by the saturated hydrogen atoms as shown in Figure S5 (ESI). For the calculation of the (hyper)polarizabilities, some deficiencies of traditional DFT methods (such as B3LYP) are not suitable to describe the electronic properties of such systems[5, 24]. In 2004, a coulomb-attenuated hybrid exchange-correlation density functional (CAM-B3LYP[67, 68]) has been developed to overcome the limitations. It is used to calculate and predict the molecular NLO properties of a few of similar systems, for example, the fullerene-dimers[69] and corresponding zig-zag BNCNTs[59-61]. In this work, results of a series of density functionals were compared to reveal the functionals effect on the first hyperpolarizabilities. The test calculation (Table 1) confirms that the β_0 of PA is the largest among the three structures, which is independent on the functionals. Considering to the computational cost and accuracy, CAM-B3LYP is adequate for our purpose according to the test results. For the basis set, the multiple-split valence basis set is capable of showing the expansion and contraction of valence atom orbitals in the molecular environment and is suitable for the calculation of the (hyper)polarizabilities[70-73]. Furthermore, the basis set effect on the β_0 is small as listed in Table S1 in Supporting Information (SI). Results show the basis effect on the β_0 of PA-6 is less than 18.5% although the basis set is significantly different. Therefore, the first hyperpolarizability is evaluated at CAM-B3LYP/6-31G* level to discuss together with corresponding electronic properties.

Table 1. The first hyperpolarizabilities (β_0) calculated by different density functionals

	PA-6	HA-6	CA-6
CAM-B3LYP	2.00×10^4	6.07×10^2	1.55×10^2
BHandHLYP	2.04×10^4	6.14×10^2	2.40×10^2
M062X	1.73×10^4	6.79×10^2	1.32×10^2
LC-BLYP	2.99×10^4	2.34×10^3	75

The polarizability (α_0) is noted as:

$$\alpha_0 = \frac{1}{3}(\alpha_{xx} + \alpha_{yy} + \alpha_{zz}) \quad (1)$$

The static first hyperpolarizability (β_0) is noted as:

$$(2)\ \beta_0 = (\beta_x^2 + \beta_y^2 + \beta_z^2)^{1/2}$$

$$\text{Where, } \beta_i = \frac{3}{5}\left(\beta_{iii} + \beta_{ijj} + \beta_{ikk}\right), i, j, k = x, y, z \quad (3)$$

All of the calculations were performed with the Gaussian 09 program package[74] except for special emphasis.

Results and Discussions

The optimized structures of the three isoelectronic models are exhibited in Figure 1 and the main bond lengths are listed in Table 2. Results show the topological structure of PA-6, HA-6 and CA-6 are similar to each other. For example, the range of C-B bond length is 1.522-1.534 **Å**. The difference of C-B bond

length among the three structures is only about 0.1 **Å**. Similarly, the C-N, B-N and C-C bond lengths of the three structures are also close to each other as listed in Table 1. On the other hand, the diameter of the tube-top (D_t) of the CA-6 is 7.161 Å, which is slightly longer than that of PA-6 or HA-6. Similar results are also shown in the comparison on diameter of the tube-bottom (D_b). It indicates that the structures of the armchair carbon-boron-nitride heterojunction nanotubes are slightly influenced by the different connecting models. However, the energy differences between the three structures indicate that electronic properties might be quite different even though the geometrical structure is similar. As shown in Table 2, the maximal difference of relative energy is about 156.88 kcal mol^{-1}.

Table 2. Main geometrical parameters (**Å**) of the three isoelectronic models optimized at the B3LYP/6-31G (d) level

	C-B	C-N	B-N	C-C	D_t	D_b	E_r
PA-6	1.534	1.391	1.426	1.439	7.119	7.119	0
HA-6	1.533	1.393	1.456	1.403	7.098	7.098	75.30
CA-6	1.522	1.415	1.449	1.413	7.161	7.041	156.88

The comparison on the electronic properties of the armchair carbon-boron-nitride heterojunction nanotubes is interesting. As shown in Table 3, the quite small difference of α_0 among the three isoelectronic models indicates that the effect of connecting pattern on polarizability is negligible. Concretely, the α_0 of CA-6 is 9.35×10^2 au, which is slightly smaller than that (1.18×10^3 au and 1.03×10^3 au) of PA-6 and HA-6. Similarly, the variation of the electronic spatial extent $<R^2>$ among the three structures is also inconspicuous (the range is 5.84×10^4-5.86×10^4). It indicates that the polarizability and the electronic spatial extent are slightly susceptible to the connecting pattern of the armchair heterojunction nanotubes. However, the difference of β_0 values among the three BNCNT models is remarkable. Results show that the β_0 value is significantly dependent on the connecting pattern of the C/BN fragment. For example, the β_0 of PA-6 is 2.00×10^4 au, which is almost two orders of magnitude higher than that (1.55×10^2 and 6.07×10^2 au) of HA-6 and CA-6. Besides, the difference of β_0 between HA-6 and CA-6 is inconspicuous even though the β_0 of PA-6 is dramatically larger. Besides, we consider other functionals to calculate corresponding electronic properties of the three models to confirm the relative magnitude. As shown in Table 1, the β_0 of PA-6 is obviously larger than the other two analogues, which is independent on the density functionals. It reveals that the β_0 of armchair BNCNT models is dramatically dependent on the connecting patterns of C/BN fragment. We are interested in the origin of the results and discuss the details as the following.

Table 3. The polarizability α_0 (a.u.) and first hyperpolarizability β_0 (a.u.) at the CAM-B3LYP/6-31G(d) level, the oscillator strength f_0 and the transition energy ΔE (eV) and the difference of dipole moment between ground state and crucial excited state ($\Delta\mu$) at the TD-CAM-B3LYP/6-31G(d)

	PA-6	HA-6	CA-6
α_0	1.18×10^3	1.03×10^3	9.35×10^2
β_x	-1.13×10^3	-4.82×10^2	1.55×10^2
β_y	1.40×10^3	99.86	0.46
β_z	1.99×10^4	-3.56×10^2	0.23
β_0	2.00×10^4	6.07×10^2	1.55×10^2
f_0	0.13	0.11	0.72
ΔE	0.83	2.76	3.52
$<R^2>$	5.84×10^4	5.86×10^4	5.84×10^4

Furthermore, the effect of C/BN formation proportion on the first hyperpolarizability of BNCNT is revealed. The β_0 of BNCNT with different formation proportion of carbon atoms are listed in Table 3. Interestingly, results show that the downtrend of β_0 is almost in the order: PA-n > HA-n > CA-n (n is the formation proportion of carbon atoms. For example, when the formation proportion is 0.2, then n is 2. Details are also shown in Figure 2 and Figure S2 in the Electronic Supplementary Information). It is worthy of note that the β_0 of CA-n almost linearly increases with the increase of carbon proportion as shown in Figure 3. For PA-n models, the β_0 significantly increases with the increase of carbon proportion when n≤6 and then slowly saturates. It indicates that the connecting patterns and formation proportion of C/BN fragment are two important factors that influence the β_0 of armchair BNCNT models. However, for HA-n models, the β_0 of HA-6 is 6.07×10^2 au, which is even smaller than 2.96×10^3 au of HA-4. The detail about the corresponding variation tendency of β_0 is discussed in the next section.

Figure 2. The CA-n models with different carbon proportion (n=2, 4, 6 and 8)

Table 4. The static first hyperpolarizability (β_0 au) of BNCNT with different connecting patterns and carbon proportion

	0.2	0.4	0.6	0.8
PA	2.39×10^3	1.02×10^4	2.00×10^4	2.02×10^4
HA	2.53×10^3	2.96×10^3	6.07×10^2	1.30×10^3
CA	0.37×10^2	1.08×10^2	1.55×10^2	1.64×10^2

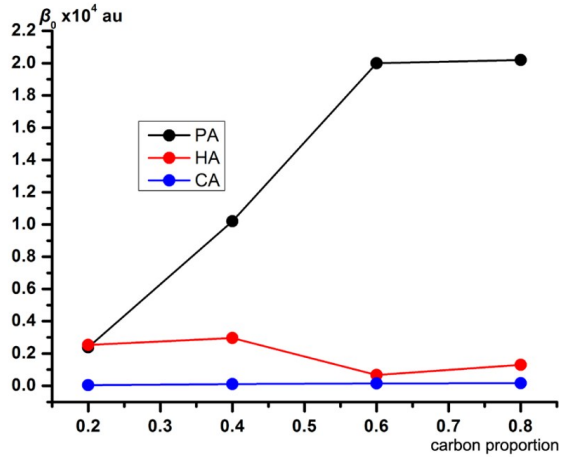

Figure 3. The relationship between the static first hyperpolarizability (β_0 au) and carbon proportion of armchair BNCNT with different connecting patterns

To get an insight into the origin of structure-property relationship of armchair BNCNT models. we consider the two-level theory proposed by Oudar and co-workers[75] to discuss the details about electronic properties. According to the two-level theory, β_0 is proportional to the oscillator strength (f_0) while inversely proportional to the third power of transition energy (ΔE^3). In this work, the corresponding properties were evaluated by time dependent (TD) CAM-B3LYP and the results are listed in Table 3. Relatively, the ΔE of PA-6 is 0.83 eV, which is remarkably lower than that (3.52 and 2.76 eV) of CA-6 and HA-6. It indicates that parallel doping the carbon segment into the armchair BNNT fragment effectively decrease the transition energy. As results, the β_0 of PA-6 is dramatically larger than that of HA-6 and CA-6. In this context, the smaller transition energy of PA-6 is the essential reason for its larger first hyperpolarizability. Correspondingly, the ΔE of HA-4 is 1.99 eV, which is obviously smaller than 2.76 eV of HA-6. As results, the β_0 of HA-4 is 2.96×10^3 au, which is larger than 6.07×10^2 au of HA-6. It is worthy of note that, different with PA-n and CA-n models, the transition nature of HA-n models is varied with the increase of carbon proportion. Therefore, the transition energy of HA-6 is larger than that of HA-4 even though the carbon proportion is larger.

Furthermore, we focused on analyzing the molecular orbitals of the important transition states to understand the origin of these properties. As shown in Figure 4, the orbitals of transition states are mainly contributed by C-segment. Therefore, the transition energy decrease with the increase of carbon proportion accompany with the increase of β_0. It is worthy of note that, a curved charge transfer is shown in PA-6. In details, the charge transfer is from the N-connecting carbon atoms to B-connecting carbon atoms, which is curvedly across the surface of PA-6. It is well known that the order of electronegativity of the three atoms is as follows: B < C < N. Correspondingly, the delocalized π-electron tends to close to

Figure 4. The most important transitions and corresponding orbital energy (eV) of CA-6, PA-6 and HA-6

the N-connecting domain in the ground state while it would close to the B-connecting domain in the excite state. Therefore, the curved charge transfer effectively decrease the transition energy of the PA-n models, which is the origin of the big difference among PA-n and CA-n (or HA-n) models. On the other hand, the total density of states (TDOS) and projected partial density of states (PDOS) have also been analyzed by the Aomix program[76, 77]. As plotted in Figure 5, both the band structure and HOMO-LUMO gap of the three models are close to each other. However, the transition nature (HOMO->LUMO) of PA-6 is significantly different with that (HOMO-3->LUMO/HOMO-4->LUMO) of CA-6/HA-6. As we mentioned in the above, it is originated from the curved charge transfer from N-connecting carbon atoms to B-connecting carbon atoms. The DOS of pristine armchair CNT and BNNT have also been shown in Figure S4 of the ESI. The energy gap of pristine BNNT is significantly larger than that of CNT. On the other hand, the energy gap of PA-6, HA-6 and CA-6 are obviously different from that of pristine BNNT but more close to pristine CNT. Compare to the pristine CNT, the participation of BN-segment in BNCNT models increase (about 0.3 eV) the energy of HOMO. It is worthy of note that the contribution of BN-segment to the main transition states in PA-6 is larger than that in HA-6 and CA-6, which decrease (about 0.5 eV) the energy of LUMO. As results, the transition energy of PA-6 is significantly smaller than that of corresponding isoelectronic models.

Figure 5. Total and partial (the BN segment and C segment) density of states (TDOS and PDOS) around the HOMO–LUMO gap

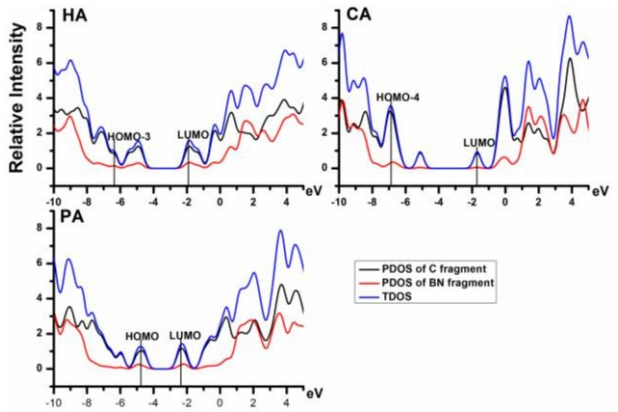

Conclusions

In summary, a series of armchair carbon-boron-nitride heterojunction nanotubes were systematically investigated to explore the physical insight of structure-property relationship. Significantly, results show that the β_0 of armchair BNCNT models is dramatically dependent on the connecting patterns and composition proportions of C/BN fragment. In detail, the β_0 value of PA-6 is 2.00×10^4 au, which is remarkably larger than that (1.55×10^2 and 6.07×10^2 au) of its isoelectronic homologues CA-6 and HA-6. Besides, the β_0 values of PA models are significantly dependent on the composition proportion of carbon atoms, whereas those of CA and HA models are slightly influenced. Further investigations on transition properties show that the curved charge transfer from N-connecting carbon atoms to B-connecting carbon atoms is the origin of the different properties between PA and CA (or HA). It is expected that the new discovery on armchair BNCNTs may provide important information for the design and preparation high performance NLO nano-materials.

Acknowledgements

The authors acknowledge the financial support from the National Science Foundation of China (Grant Nos. 21473026, 21573089), the Science and Technology Development Planning of Jilin Province (20140101046JC).

Notes and references

1 Y. R. Shen, *Wiley: NewYork*, 1984.
2 D. R. Kanis, M. A. Ratner and T. J. Marks, *Chem. Rev.*, 1994, **94**, 195-242.
3 D. F. Eaton, *Science*, 1991, **253**, 281-287.
4 B. J. Coe, *Acc. Chem. Res.*, 2006, **39**, 383-393.
5 B. Champagne, E. A. Perpète, D. Jacquemin, S. J. A. van Gisbergen, E.-J. Baerends, C. Soubra-Ghaoui, K. A. Robins and B. Kirtman, *J. Phys. Chem. A*, 2000, **104**, 4755-4763.
6 S. Muhammad, H.-L. Xu, R.-L. Zhong, Z.-M. Su, A. G. Al-Sehemi and A. Irfan, *J. Mater. Chem. C*, 2013, **1**, 5439-5449.
7 M. Nakano, T. Minami, K. Yoneda, S. Muhammad, R. Kishi, Y. Shigeta, T. Kubo, L. a. Rougier, B. t. Champagne, K. Kamada and K. Ohta, *J. Phys. Chem. Lett.*, 2011, **2**, 1094-1098.
8 B. Champagne, *Chem. Modell.*, 2009, 17-62.
9 M. Luo, G. Wang, C. Lin, N. Ye, Y. Zhou and W. Cheng, *Inorg. Chem.*, 2014, **53**, 8098-8104.
10 G. Zou, L. Huang, N. Ye, C. Lin, W. Cheng and H. Huang, *J. Am. Chem. Soc.*, 2013, **135**, 18560-18566.
11 G. Wang, M. Luo, C. Lin, N. Ye, Y. Zhou and W. Cheng, *Inorg. Chem.*, 2014, **53**, 12584-12589.
12 W. Lin, L. Ma and O. R. Evans, *Chem. Commun.*, 2000, 2263-2264.
13 O. R. Evans and W. Lin, *Acc. Chem. Res.*, 2002, **35**, 511-522.
14 B. Champagne, E. Botek, M. Nakano, T. Nitta and K. Yamaguchi, *J. Chem. Phys.*, 2005, **122**, 114315-114312.
15 S. R. Marder, D. N. Beratan and L.-T. Cheng, *Science*, 1991, **252**, 103-106.
16 B. J. Coe, *Coord. Chem. Rev.*, 2013, **257**, 1438-1458.
17 B. J. Coe, S. P. Foxon, M. Helliwell, D. Rusanova, B. S. Brunschwig, K. Clays, G. Depotter, M. Nyk, M. Samoc, D. Wawrzynczyk, J. Garin and J. Orduna, *Chem. Eur. J.*, 2013, **19**, 6613-6629.
18 W. Chen, Z.-R. Li, D. Wu, Y. Li, C.-C. Sun and F. L. Gu, *J. Am. Chem. Soc.*, 2005, **127**, 10977-10981.
19 W. Chen, Z.-R. Li, D. Wu, Y. Li, C.-C. Sun, F. L. Gu and Y. Aoki, *J. Am. Chem. Soc.*, 2006, **128**, 1072-1073.
20 H.-L. Xu, Z.-R. Li, D. Wu, B.-Q. Wang, Y. Li, F. L. Gu and Y. Aoki, *J. Am. Chem. Soc.*, 2007, **129**, 2967-2970.
21 S. Muhammad, H. Xu, Y. Liao, Y. Kan and Z. Su, *J. Am. Chem. Soc.*, 2009, **131**, 11833-11840.
22 S. Muhammad, H. Xu and Z. Su, *J. Phys. Chem. A*, 2011, **115**, 923-931.
23 R.-L. Zhong, H.-L. Xu, Z.-R. Li and Z.-M. Su, *J. Phys. Chem. Lett.*, 2015, **6**, 612-619.
24 D. Xiao, F. A. Bulat, W. Yang and D. N. Beratan, *Nano Lett.*, 2008, **8**, 2814-2818.
25 F. Ma, Z.-J. Zhou, Z.-R. Li, D. Wu, Y. Li and Z.-S. Li, *Chem. Phys. Lett.*, 2010, **488**, 182-186.
26 H.-L. Xu, F.-F. Wang, Z.-R. Li, B.-Q. Wang, D. Wu, W. Chen, G.-T. Yu, F. L. Gu and Y. Aoki, *J. Comput. Chem.*, 2009, **30**, 1128-1134.
27 H.-L. Xu, R.-L. Zhong, S.-L. Sun and Z.-M. Su, *J. Phys. Chem. C*, 2011, **115**, 16340-16346.
28 S. Enouz, O. Stéphan, J.-L. Cochon, C. Colliex and A. Loiseau, *Nano Lett.*, 2007, **7**, 1856-1862.
29 W. Lu, M. Zu, J.-H. Byun, B.-S. Kim and T.-W. Chou, *Adv. Mater.*, 2012, **24**, 1805-1833.
30 J. M. Schnorr and T. M. Swager, *Chem. Mater.*, 2010, **23**, 646-657.
31 Y. Zhang, Y. Song, Y. Gan, M. Feng and H. Zhan, *J. Mater. Chem. C*, 2015, **3**, 9948-9954.
32 Z.-B. Liu, Z.-J. Zhou, Z.-R. Li, Q.-Z. Li, F.-Y. Jia, J.-B. Cheng and C.-C. Sun, *J. Mater. Chem.*, 2011, **21**, 8905-8910.
33 N. G. Chopra, R. J. Luyken, K. Cherrey, V. H. Crespi, M. L. Cohen, S. G. Louie and A. Zettl, *Science*, 1995, **269**, 966-967.
34 D. Golberg, Y. Bando, C. C. Tang and C. Y. Zhi, *Adv. Mater.*, 2007, **19**, 2413-2432.
35 C. Y. Zhi, Y. Bando, C. C. Tang, Q. Huang and D. Golberg, *J. Mater. Chem.*, 2008, **18**, 3900-3900.
36 X. Wei, D.-M. Tang, Q. Chen, Y. Bando and D. Golberg, *ACS Nano*, 2013, **7**, 3491-3497.
37 J. Zhao, W. Li, C. Tang, L. Li, J. Lin and C. Gu, *Appl. Phys. Lett.*, 2013, **102**, 153107-153104.
38 X. Zhong, S. Mukhopadhyay, S. Gowtham, R. Pandey and S. P. Karna, *Appl. Phys. Lett.*, 2013, **102**, 133705-133704.

39 D. Golberg, Y. Bando, Y. Huang, T. Terao, M. Mitome, C. Tang and C. Zhi, *ACS Nano*, 2010, **4**, 2979-2993.
40 J. Choi, Y.-H. Kim, K. J. Chang and D. Tománek, *Phys. Rev. B*, 2003, **67**, 125421.
41 X. Wei, M.-S. Wang, Y. Bando and D. Golberg, *ACS Nano*, 2011, **5**, 2916-2922.
42 G. Y. Guo and J. C. Lin, *Phys. Rev. B*, 2005, **72**.
43 R. Orlando, R. Bast, K. Ruud, U. Ekström, M. Ferrabone, B. Kirtman and R. Dovesi, *J. Phys. Chem. A*, 2011, **115**, 12631-12637.
44 A. Erba, M. Ferrabone, J. Baima, R. Orlando, M. Rérat and R. Dovesi, *J. Chem. Phys.*, 2013, **138**, 054906.
45 A. Mohajeri and A. Omidvar, *J. Phys. Chem. C*, 2014, **118**, 1739-1745.
46 R.-L. Zhong, H.-L. Xu, S.-L. Sun, Y.-Q. Qiu and Z.-M. Su, *Chem. Eur. J.*, 2012, **18**, 11350-11355.
47 R.-L. Zhong, H.-L. Xu, S. Muhammad, J. Zhang and Z.-M. Su, *J. Mater. Chem.*, 2012, **22**, 2196-2202.
48 O. Stephan, P. M. Ajayan, C. Colliex, P. Redlich, J. M. Lambert, P. Bernier and P. Lefin, *Science*, 1994, **266**, 1683-1685.
49 Z. Weng-Sieh, K. Cherrey, N. G. Chopra, X. Blase, Y. Miyamoto, A. Rubio, M. L. Cohen, S. G. Louie, A. Zettl and R. Gronsky, *Phys. Rev. B*, 1995, **51**, 11229-11232.
50 V. V. Ivanovskaya, A. Zobelli, O. Stéphan, P. R. Briddon and C. Colliex, *J. Phys. Chem. C*, 2009, **113**, 16603-16609.
51 A. Du, Y. Chen, Z. Zhu, G. Lu and S. C. Smith, *J. Am. Chem. Soc.*, 2009, **131**, 1682-1683.
52 Z.-Y. Zhang, Z. Zhang and W. Guo, *J. Phys. Chem. C*, 2009, **113**, 13108-13114.
53 B. Huang, C. Si, H. Lee, L. Zhao, J. Wu, B.-L. Gu and W. Duan, *Appl. Phys. Lett.*, 2010, **97**, 043115-043113.
54 M. M. Wu, X. Zhong, Q. Wang, Q. Sun, R. Pandey and P. Jena, *J. Phys. Chem. C*, 2011, **115**, 23978-23983.
55 J. M. Pruneda, *Phys. Rev. B*, 2012, **85**, 045422.
56 M. Machado, T. Kar and P. Piquini, *Nanotechnology*, 2011, **22**, 205706-205706.
57 A. A. El-Barbary, K. M. Eid, M. A. Kamel and M. M. Hassan, *Comp. Mater. Sci.*, 2013, **69**, 87-94.
58 W. An and C. H. Turner, *J. Phys. Chem. Lett.*, 2010, **1**, 2269-2273.
59 R.-L. Zhong, S.-L. Sun, H.-L. Xu, Y.-Q. Qiu and Z.-M. Su, *J. Phys. Chem. C*, 2013, **117**, 10039-10044.
60 R.-L. Zhong, S.-L. Sun, H.-L. Xu, Y.-Q. Qiu and Z.-M. Su, *J. Phys. Chem. C*, 2014, **118**, 14185-14191.
61 R.-L. Zhong, S.-L. Sun, H.-L. Xu, Y.-Q. Qiu and Z.-M. Su, *ChemPlusChem*, 2014, **79**, 732-736.
62 Z. Guan, W. Wang, J. Huang, X. Wu, Q. Li and J. Yang, *J. Phys. Chem. C*, 2014, **118**, 28616-28624.
63 J. Gu, Y.-Q. Le, Y.-Y. Hu, W.-Q. Li and W. Q. Tian, *ACS Photonics*, 2014, **1**, 928-935.
64 Y. Morita, S. Suzuki, K. Sato and T. Takui, *Nat Chem*, 2011, **3**, 197-204.
65 A. D. Becke, *J. Chem. Phys.*, 1993, **98**, 5648-5652.
66 A. D. Becke, *J. Chem. Phys.*, 1993, **98**, 1372-1377.
67 H. Iikura, T. Tsuneda, T. Yanai and K. Hirao, *J. Chem. Phys.*, 2001, **115**, 3540-3544.
68 T. Yanai, D. P. Tew and N. C. Handy, *Chem. Phys. Lett.*, 2004, **393**, 51-57.
69 F. Ma, Z.-R. Li, Z.-J. Zhou, D. Wu, Y. Li, Y.-F. Wang and Z.-S. Li, *J. Phys. Chem. C*, 2010, **114**, 11242-11247.
70 G. Maroulis, D. Xenides, U. Hohm and A. Loose, *J. Chem. Phys.*, 2001, **115**, 7957-7967.
71 P. Karamanis and G. Maroulis, *Chem. Phys. Lett.*, 2003, **376**, 403-410.
72 P. Karamanis and G. Maroulis, *J. Mol. Struct.: THEOCHEM*, 2003, **621**, 157-162.
73 G. Maroulis, *J. Chem. Phys.*, 2008, **129**, 044314.
74 M. J. Frisch and e. a. G. W. Trucks.
75 J. L. Oudar and D. S. Chemla, *J. Chem. Phys.*, 1977, **66**, 2664-2668.
76 S. I. Gorelsky and A. B. P. Lever, *J. Organomet. Chem.*, 2001, **635**, 187-196.
77 S. I. Gorelsky, 2009 AOMix: Program for Molecular Orbital Analysis, University of Ottawa.